http://dx.doi.org/10.5012/bkcs.2013.34.5.1551

Theoretical Investigation of the Reaction of Ce^+ with Water in the Gas Phase: Density Functional Theory Calculations

Kiryong Hong, Joonghan Kim,†,* and Tae Kyu Kim*

Department of Chemistry and Chemical Institute for Functional Materials, Pusan National University, Busan 609-735, Korea
**E-mail: tkkim@pusan.ac.kr*
*†Department of Chemistry, The Catholic University of Korea, Bucheon 420-743, Korea. *E-mail: joonghankim@catholic.ac.kr*
Received December 31, 2012, Accepted February 19, 2013

Key Words : Lanthanide ion, Water, Density functional calculation, Reaction mechanism

The importance of rare earth elements is growing in many areas, especially chemical catalysis,[1,2] metallurgy[3] and industrial field.[4] Accordingly, gas-phase reactions of various organic compounds with lanthanide cations have been extensively investigated by spectroscopic experiments[5-10] and computational studies[11-13] for decades. Among these molecular systems, H_2O as the simplest molecule having the O–H bond, serves as a good model to understand the O–H bond activation by lanthanide cations. For example, the reactions of H_2O with many metal mono-cations have been plentifully investigated experimentally[7,14,15] and theoretically.[16-19]

Cheng *et al*. performed the experiments on the reactions of various 29 transition metal ions, 17 main-group atomic ions and all lanthanide ions except Pm^+ with D_2O by using the inductively coupled plasma/selected-ion flow tube (ICP/SIFT) tandem mass spectrometry.[7,15] Their experimental results showed that the reactions proceeded to one of the ensuing channels: (1) O atom transfer ($M^+ + D_2O \rightarrow MO^+ + D_2$), (2) OD transfer ($M^+ + D_2O \rightarrow MOD^+ + D$), and (3) D_2O molecular addition ($M^+ + D_2O \rightarrow M^+OD_2$). The reactions of 3*d* transition metal ions with H_2O have been studied theoretically by Irigoras and co-workers[16-19] and their calculated results have shown that the most favorable reaction pathway of the reactions involving early transition metal ions (Sc^+, Ti^+, and V^+)[17,19] was the O atom transfer but those involving middle (Cr^+, Mn^+, and Fe^+)[18] and late transition metal ions (Co^+, Ni^+, and Cu^+)[16] was H_2O molecular addition. These results are in good agreement with Cheng's experimental results.[15]

Although a number of studies for the reactions of various metal ions with H_2O have been investigated, theoretical investigations for the reactions of lanthanide ions such as Ce^+ with H_2O have not been carried out. Several experimental investigations by Cheng *et al*.[7,15] have shown that the reaction of Ce^+ with H_2O go through following the O atom transfer pathways. The detailed reaction mechanism Ce^+ with H_2O has not been explained yet. In addition, Ce^+ may serve as a good model to understand covalent and ionic chemical bonds between lanthanide and main group atoms because the ground electronic configuration of Ce^+ involves 5*d* orbital occupations as well as 4*f* occupation. Thus, theoretical investigation involving the detailed reaction mechanisms of Ce^+ with H_2O is demanded to elucidate the reaction mechanisms. For this purpose, in this work, we have examined all possible reaction species, occurring on the reaction potential energy surfaces (PESs) of Ce^+ with H_2O using the density functional theory (DFT) method.[20,21] In addition, the intersystem crossing (ISC) point is estimated by the single-point energy calculations along the reaction pathway. These results correlated to the recent experimental findings.[7,15]

We calculated the doublet and quartet PESs for the ion-molecule reaction of Ce^+ with H_2O using DFT method, since these two states are very close in energy and may interconvert during the reaction. All molecular structures of the reaction species (reactants, intermediates, products, and transition states) were fully optimized using PBE0 hybrid DFT functional,[22] which are frequently used and gives reasonable results for lanthanide molecular systems.[23-25] The unrestricted formalism (UPBE0) was used for all spin states. In particular, an open shell structure was used for the singlet spin states. We used the relativistic effective core potential (RECP) to treat the scalar relativistic effect for the lanthanide ion, Ce^+. The small-core Stuttgart ECP28MWB[26,27] with the large atomic natural orbital (ANO) valence basis set ([6*s*6*p*5*d*4*f*3*g*]) and 6-311++G(d,p) basis sets were used for the lanthanide ion (Ce^+) and other atoms (H and O), respectively. We also carried out the harmonic vibrational frequency calculation. All transition states were identified by one imaginary frequency and confirmed by using the intrinsic reaction coordinate (IRC) method.[28,29] All relative energies included the zero-point energy (ZPE) correction for all reaction species. We also used the natural population analysis (NPA)[30] for characterizing atomic charge and electronic structure. All calculations were carried out using the Gaussian 03 program.[31]

All optimized geometries of both doublet and quartet spin states and the reaction PESs regarding to the reactions of Ce^+ with H_2O are shown in Figures 1 and 2, respectively. The initiation step of the reaction is the association complex formation in both spin states. As shown in Figure 1, Ce^+ moves toward the electron rich oxygen atom of the water to form an initial intermediate, IM_1 in both spin states. This result can be readily expected due to the electronegativity of

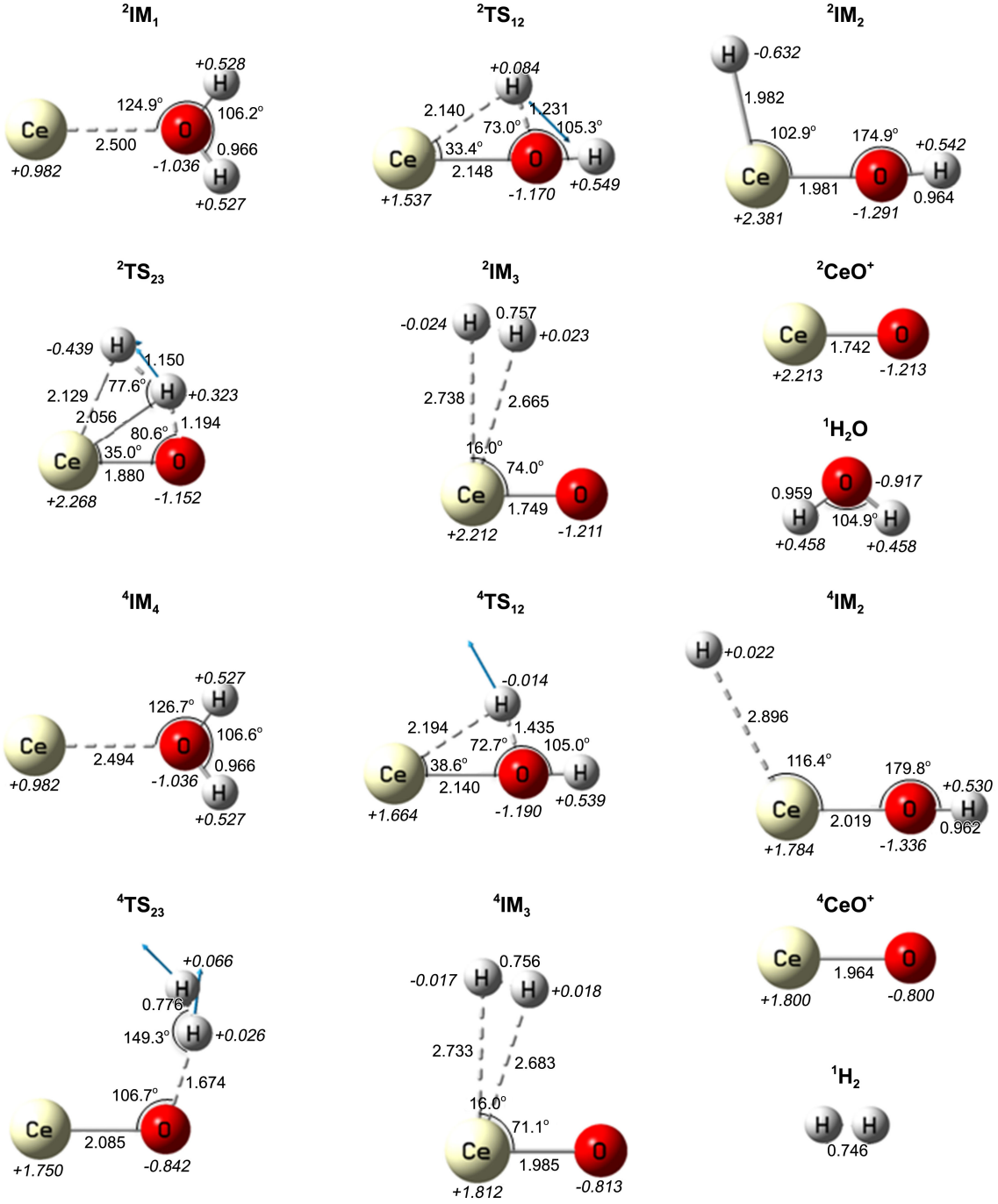

Figure 1. Selected parameters (bond lengths in Å and bond angles in degree) of optimized molecular strucutures of the reactant (H_2O), the products (CeO^+ and H_2), the intermediates (IMs), and the transition states (TSs) calculated by UPBE0 functional on the reaction of Ce^+ with H_2O. NPA charges are displayed in italic numbers. Blue arrows indicate the transition vectors of main atomic motions in the transition states.

the O atom in water. In both $^2IM_1$ and $^4IM_1$ (the superscript denotes the spin multiplicity) structures, the Ce–O bonds are almost pure ionic bond according to NPA charge of Ce atom, which are the same value (+0.982) in both structures. In addition, Ce^+ in both $^2IM_1$ and $^4IM_1$ structure has the same molecular orbital (MO) character as those of $^2Ce^+$ and $^4Ce^+$, respectively. These results can clarify why both $^2IM_1$ and $^4IM_1$ structures have similar geometrical parameters (see Figure 1). As shown in Figure 2, the $^2IM_1$ lies slightly higher in energy (3.9 kcal/mol) than $^4IM_1$. This energy difference is similar to that between $^2Ce^+$ and $^4Ce^+$ (2.7 kcal/mol). This result can also be attributed to the same electronic configuration of Ce^+ between bare ions and those of IM_1 structure.

After the complexation, Ce^+ abstracts one H atom from the water *via* the transition state, TS_{12} in both doublet and quartet spin states, namely, Ce^+ activates the O–H bond of H_2O. The NPA charges of Ce in both $^2TS_{12}$ and $^4TS_{12}$ structures are +1.537 and +1.664, respectively; these values are

different from those of both $^2IM_1$ and $^4IM_1$ structures (+0.982 for both). These results indicate that the electronic structure of Ce changes through the H abstraction, suggesting the covalent contribution (orbital overlaps between *d* orbital of Ce and *p* orbital of O and between *d* orbital of Ce and *s* orbital of H) increases. Generally, a tunneling plays an important role in the H transfer step (from O to Ce in this case). The tunneling probability significantly increases as a barrier height decreases. In this reaction, the barrier heights are 13.3 and 16.6 kcal/mol on $^2TS_{12}$ and $^4TS_{12}$, respectively. Since both barrier heights are considerable, the tunneling effect is insignificant in this H transfer step.

After the H abstraction by Ce^+, the distance between Ce and H is significantly different from each other; the Ce–H distance (2.896 Å) of $^4IM_2$ structure much longer than that (1.982 Å) of $^2IM_2$ structure (see Figure 1). The NPA charges of Ce and H (Ce: +1.784 and H: +0.022) in the $^4IM_2$ structure show that no bond between Ce and H exists. Indeed, no orbital overlap between Ce and H on $^4IM_2$ has been observed. Three unpaired electrons occupy *d* and *f* orbitals of Ce and *s* orbital of H in the $^4IM_2$ structure. In contrast, the strong overlap between *d* orbital of Ce and *s* orbital of H exists in the $^2IM_2$ structure. In addition, two α and β electrons occupy the bonding orbital between Ce and H (one unpaired electron occupies the non-bonding f orbital of Ce in the $^2IM_2$ structure). Thus, the short bond length of Ce–H (1.982 Å) in the $^2IM_2$ structure is attributed to this electronic configuration.

The electronic structure dramatically changed as the reaction proceeds from TS_{12} to IM_2. As mentioned above, the electronic structure of $^2IM_2$ is quite different from that of $^4IM_2$. In the $^2IM_2$ structure, especially, two paired electrons occupy the bonding molecular orbital of Ce–H. This electronic structure results in the stabilization of the $^2IM_2$ structure compared with the $^4IM_2$ as shown in Figure 2. Moreover, it should be noted that the oxidation number of Ce has become +3 in the $^2IM_2$ structure. The favor of +3 oxidation number is well-known property for the lanthanide atoms. This result can also elucidate sharp energy lowering of the $^2IM_2$. The +3 oxidation number of Ce on the doublet spin state has been kept up to the product. As shown in Figure 2, the stabilization of the $^2IM_2$ also leads to the reversal of energy ordering; the $^4IM_2$ lies much higher in energy than the $^2IM_2$. This indicates that the intersystem crossing between the doublet and quartet PESs should exist. We have estimated the location of ISC between quartet and doublet spin states *via* the single-point calculations along IRC pathway of doublet state (from $^2TS_{12}$ to $^2IM_2$). The two diabatic PESs (doublet and quartet) are shown in Figure 3 and the crossing point of two PESs is also clearly seen. Although actual adiabatic PESs should be calculated including spin-orbit coupling (SOC), we can easily expect that the spin state readily changes due to intrinsic large SOC of lanthanide atom. Once the spin state changes from quartet to doublet as shown in Figure 3, the $^2IM_2$ is thermochemically much more stable than $^4IM_2$. In other words, the reaction can proceed from $^4TS_{12}$ (quartet) to $^2IM_2$ (doublet) with thermochemical stability which is induced by large SOC of Ce.

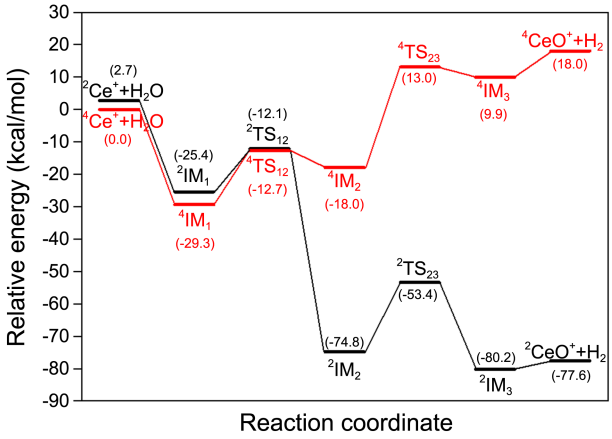

Figure 2. Reaction PESs in doublet and quartet spin states for the reaction of Ce^+ with H_2O calculated by UPBE0 functional. Values in parentheses are the relative energies and the superscript denotes the spin multiplicity.

In the next step, two hydrogen atoms of IM_2 are close to each other through TS_{23}. However, as shown in Figure 1, the structure of $^2TS_{23}$ is quite different from $^4TS_{23}$. The H–H bond distance of $^2TS_{23}$ is 1.150 Å, on the other hands, that of $^4TS_{23}$ is only 0.776 Å, which is close to H–H bond length of H_2 molecule, 0.746 Å. Furthermore, Ce–O (1.880 Å for $^2TS_{23}$ and 2.085 Å for $^4TS_{23}$) and O–H distances (1.194 Å for $^2TS_{23}$ and 1.674 Å for $^4TS_{23}$) are quite different in two TS_{23}. In the $^2TS_{23}$ structure, the covalent bond between Ce and H still exist although its bond length is longer than that of $^2IM_2$. As can be seen in Figure S1(a), the orbital overlaps between Ce and H in the $^2TS_{23}$ structure exist. In contrast, in the $^4TS_{23}$ structure, no orbital overlap between them is observed (see Figure S1(b)). In addition, H_2 molecule almost forms according to its bond length and NPA charges whose sum (0.089) is close to 0 in the $^4TS_{23}$ structure. However, in the $^2TS_{23}$ structure, extra charge (0.439 + 0.323 = –0.116, see Figure 1) of H_2 exists, which occupy σ* orbital of H_2 molecule resulting in elongation of bond length (1.150 Å). In this step, namely, H_2 formation step, no role of Ce is in the quartet spin state ($^4TS_{23}$); only O mediates the H_2 formation. On the contrary, Ce in the $^2TS_{23}$ structure mediates the H_2 formation *via* covalent contribution of 5*d* and 4*f* orbitals of Ce. These contributions lead to the lowering of activation barrier for this step. As shown in Figure 2, the H_2 formation step (from IM_2 to TS_{23}) is the rate determining step on both spin states. The activation barrier of the doublet state is 21.4 kcal/mol which is smaller than that (31.0 kcal/mol) of the quartet spin state. Therefore, Ce catalyzes the H_2 formation and its magnitude of lowering is about 10 kcal/mol.

As a final step of titled reaction, H_2 forms on both $^2IM_3$ and $^4IM_3$ structures. The distances between H_2 and Ce are very long and the geometrical parameters of both $^2IM_3$ and $^4IM_3$ are similar to each other except CeO bond length, indicating that H_2 unit is separated from CeO unit. The NPA charges of H_2 in both $^2IM_3$ and $^4IM_3$ structures also confirm that (see Figure 1). Finally, on both spin states, H_2 are getting

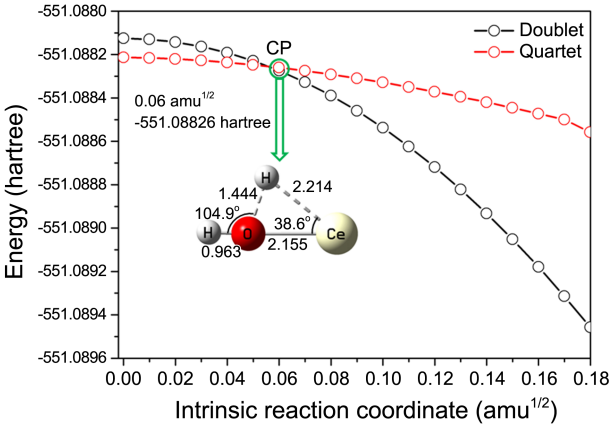

Figure 3. Single-point energies of quartet state related with the crossing point (CP) along the doublet state PES (IRC pathway from $^2TS_{12}$ to $^2IM_2$) of the reaction of Ce^+ with H_2O.

far away from CeO without barrier and the reactions are completed. It is worthwhile to mention two major roles of Ce in the reaction of Ce^+ with H_2O. First, the two spin states (doublet and quartet) are mixed due to large SOC of Ce and the reaction proceeds from the quartet to doublet spin state where thermochemically is stable. Second, the activation barrier of the H_2 formation, the rate-determining step, has been reduced due to the mediation of Ce. Thus, the O atom transfer reaction can be readily occurred because of the crucial roles of Ce. This result is in good agreement with the recent experimental finding.

In summary, we have performed DFT calculations to elucidate the reaction mechanism of reaction Ce^+ with H_2O. Our calculated PESs in both doublet and quartet spin states account for how Ce^+ activates the OH bond of water in the gas phase and subsequently generates CeO^+ and H_2 products in details. The efficiency of this reaction can be attributed to two major role of Ce^+. First, the spin multiplicity changes from the quartet to doublet due to SOC of Ce atom. Second, Ce catalyzes the H_2 formation step, rate determining step due to the covalent contribution of 5*d* orbital of Ce atom. The calculated results well explain the experimental findings.

Acknowledgments. This work was financially supported by the Research Fund Program of Research Institute for Basic Science, Pusan National University, Korea, 2008, Project No. RIBS-PNU-2008-102.

Supporting Information. Selective molecular orbitals of $^2TS_{23}$ and $^4TS_{23}$. This supporting material may be found in the online version of this article.

References

1. Sasai, H.; Suzuki, T.; Arai, S.; Arai, T.; Shibasaki, M. *J. Am. Chem. Soc.* **1992**, *114*, 4418.
2. Hattori, H. *Chem. Rev.* **1995**, *95*, 537.
3. Gupta, C. K.; Krishnamurthy, N. *Extractive Metallurgy of Rare Earths*; CRC Press: Boca Raton, Florida., 2005.
4. Karl, A.; Gschneidner, J. *Industrial Applications of Rare Earth Elements*; American Chemical Society: Washington, DC, 1981.
5. Cornehl, H. H.; Hornung, G.; Schwarz, H. *J. Am. Chem. Soc.* **1996**, *118*, 9960.
6. Lavrov, V. V.; Blagojevic, V.; Koyanagi, G. K.; Orlova, G.; Bohme, D. K. *J. Phys. Chem. A* **2004**, *108*, 5610.
7. Cheng, P.; Koyanagi, G. K.; Bohme, D. K. *Chem. Phys. Chem.* **2006**, *7*, 1813.
8. Cheng, P.; Koyanagi, G. K.; Bohme, D. K. *J. Phys. Chem. A* **2006**, *110*, 12832.
9. Bandura, D. R.; Baranov, V. I.; Litherland, A. E.; Tanner, S. D. *Int. J. Mass Spectrom.* **2006**, *255-256*, 312.
10. Koyanagi, G. K.; Zhao, X.; Blagojevic, V.; Jarvis, M. J. Y.; Bohme, D. K. *Int. J. Mass Spectrom.* **2005**, *241*, 189.
11. Zhang, D.; Zhang, C.; Liu, C. *J. Organomet. Chem.* **2001**, *640*, 121.
12. Wang, Y.-C.; Liu, Z.-Y.; Geng, Z.-Y.; Yang, X.-Y.; Gao, L.-G.; Chen, X.-X. *J. Mol. Struct. (THEOCHEM)* **2006**, *765*, 27.
13. Zhang, D.; Liu, C.; Bi, S. *J. Phys. Chem. A* **2002**, *106*, 4153.
14. Jackson, G. P.; King, F. L.; Goeringer, D. E.; Duckworth, D. C. *J. Phys. Chem. A* **2002**, *106*, 7788.
15. Cheng, P.; Koyanagi, G. K.; Bohme, D. K. *J. Phys. Chem. A* **2007**, *111*, 8561.
16. Irigoras, A.; Elizalde, O.; Silanes, I.; Fowler, J. E.; Ugalde, J. M. *J. Am. Chem. Soc.* **2000**, *122*, 114.
17. Irigoras, A.; Fowler, J. E.; Ugalde, J. M. *J. Am. Chem. Soc.* **1999**, *121*, 574.
18. Irigoras, A.; Fowler, J. E.; Ugalde, J. M. *J. Am. Chem. Soc.* **1999**, *121*, 8549.
19. Irigoras, A.; Fowler, J. E.; Ugalde, J. M. *J. Phys. Chem. A* **1998**, *102*, 293.
20. Hohenberg, P.; Kohn, W. *Phys. Rev.* **1964**, *136*, B864.
21. Kohn, W.; Sham, L. J. *Phys. Rev.* **1965**, *140*, A1133.
22. Adamo, C.; Barone, V. *J. Chem. Phys.* **1999**, *110*, 6158.
23. Adamo, C.; Barone, V. *J. Comput. Chem.* **2000**, *21*, 1153.
24. Pantazis, D. A.; Neese, F. *J. Chem. Theory Comput.* **2009**, *5*, 2229.
25. Dolg, M. *J. Chem. Theory Comput.* **2011**, *7*, 3131.
26. Dolg, M.; Stoll, H.; Preuss, H. *J. Chem. Phys.* **1989**, *90*, 1730.
27. Cao, X.; Dolg, M. *J. Chem. Phys.* **2001**, *115*, 7348.
28. Gonzalez, C.; Schlegel, H. B. *J. Chem. Phys.* **1989**, *90*, 2154.
29. Gonzalez, C.; Schlegel, H. B. *J. Phys. Chem.* **1990**, *94*, 5523.
30. Reed, A. E.; Weinstock, R. B.; Weinhold, F. *J. Chem. Phys.* **1985**, *83*, 735.
31. Frisch, M. J.; Trucks, G. W.; Schlegel, H. B.; Scuseria, G. E.; Robb, M. A.; Cheeseman, J. R.; Montgomery, J. A.; Vreven, T.; Kudin, K. N.; Burant, J. C.; Millam, J. M.; Iyengar, S. S.; Tomasi, J.; Barone, V.; Mennucci, B.; Cossi, M.; Scalmani, G.; Rega, N.; Petersson, G. A.; Nakatsuji, H.; Hada, M.; Ehara, M.; Toyota, K.; Fukuda, R.; Hasegawa, J.; Ishida, M.; Nakajima, T.; Honda, Y.; Kitao, O.; Nakai, H.; Klene, M.; Li, X.; Knox, J. E.; Hratchian, H. P.; Cross, J. B.; Adamo, C.; Jaramillo, J.; Gomperts, R.; Stratmann, R. E.; Yazyev, O.; Austin, A. J.; Cammi, R.; Pomelli, C.; Ochterski, J. W.; Ayala, P. Y.; Morokuma, K.; Voth, G. A.; Salvador, P.; Dannenberg, J. J.; Zakrzewski, V. G.; Dapprich, S.; Daniels, A. D.; Strain, M. C.; Farkas, O.; Malick, D. K.; Rabuck, A. D.; Raghavachari, K.; Foresman, J. B.; Ortiz, J. V.; Cui, Q.; Baboul, A. G.; Clifford, S.; Cioslowski, J.; Stefanov, B. B.; Liu, G.; Liashenko, A.; Piskorz, P.; Komaromi, I.; Martin, R. L.; Fox, D. J.; Keith, T.; Al-Laham, M. A.; Peng, C. Y.; Nanayakkara, A.; Challacombe, M.; Gill, P. M. W.; Johnson, B.; Chen, W.; Wong, M. W.; Gonzalez, C.; Pople, J. A.; Gaussian 03, Revision C.02 ed.; Gaussian, Inc.: Wallingford CT, 2004.